Powder Technology 449 (2025) 120346

Contents lists available at ScienceDirect

Powder Technology

journal homepage: www.journals.elsevier.com/powder-technology

Direct observation of particle clustering and gas breakdown in charged granular streams

Yifan Wang [a,b,1], Meng Yang [a,1], Zhicheng Wu [a], Lingyu Shao [a], Libin Yu [c], Yongxin Zhang [a,b,d], Zhengda Yang [e], Yingchun Wu [a], Chenghang Zheng [a,b,c,d,*], Xiang Gao [a,b,c,d,*]

[a] State Key Laboratory of Clean Energy Utilization, State Environmental Protection Engineering Center for Coal-Fired Air Pollution Control, Zhejiang University, Hangzhou 310027, People's Republic of China
[b] Institute of Carbon Neutrality, Zhejiang University, Hangzhou 310027, People's Republic of China
[c] Zhejiang Baima Lake Laboratory Co., Ltd., Hangzhou 310051, People's Republic of China
[d] Jiaxing Research Institute, Zhejiang University, Jiaxing 314000, People's Republic of China
[e] College of New Energy, China University of Petroleum (East China), Qingdao 266580, People's Republic of China

HIGHLIGHTS

- The deposition performance of charged particle in electric field was discussed.
- The process of particle clustering and gas breakdown was directly observed.
- The particle charging and migration performance were systematically explored.
- The countermeasures for inhibiting gas breakdown and re-entrainment were proposed.

GRAPHICAL ABSTRACT

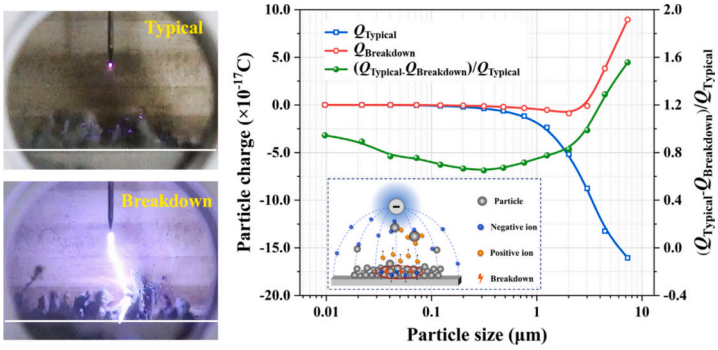

ARTICLE INFO

Keywords:
Dust layer
Gas breakdown
Chain agglomerates
Particle charging
Collection efficiency

ABSTRACT

The dust layer formed by charged particles deposition significantly limit the collection efficiency and stable application of electrostatic precipitators (ESPs). However, the deposition characteristics and re-entrainment mechanism of charged particles in electric field still remain unclear. In this study, a transparent ESP was designed to investigate the dynamic process of charged particle deposition, clustering and gas breakdown in electric field. The results showed that deposited particles will aggregate and gradually grow in chains in high-voltage electric field. The length of chain agglomerates can exceed 10 mm. And interelectrode gas breakdown could suddenly occur, which significantly changed the particle charging characteristics and increased particle emission at the outlet. In addition, a perforated plate was proposed to inhibit the gas breakdown and particle re-entrainment. The mass concentrations of particle re-entrainment decreased by 85.2 % and 79.1 % for the spike electrode and the arista electrode at the applied voltage of 30 kV, respectively.

* Corresponding authors at: State Key Lab of Clean Energy Utilization, Institute for Thermal Power Engineering, Zhejiang University, Hangzhou 310027, People's Republic of China.
E-mail addresses: zhengch2003@zju.edu.cn (C. Zheng), xgao1@zju.edu.cn (X. Gao).
[1] These authors contributed equally to this work.

https://doi.org/10.1016/j.powtec.2024.120346
Received 15 August 2024; Received in revised form 2 October 2024; Accepted 6 October 2024
Available online 9 October 2024

1. Introduction

Various pollutants are emitted in the processes of energy utilization, where particulate matter (PM) has attracted widespread attention due to its harmful effects on human health and ecological environment [1–3]. Especially, $PM_{2.5}$ pollutants can get into human lungs and cause severe damage to the human respiratory system [4–6]. In recent years, many countries have issued stricter emission limitations for particulate matter emissions to satisfy the requirements of environmental sustainability [7–9].

Electrostatic precipitator (ESP) is one of the most widely used and technologically mature methods for PM control [10–12], and its particle removal efficiency can be up to 99.9 % under ideal conditions [13,14]. Inside an ESP, the flue gas can be ionized during the corona discharge process for particle charging [15–18]. Afterwards, the charged particles are separated from the flue gas and gradually deposited on the collection plate under the action of the electric field [19–21], forming a dust layer with increasing thickness. However, the ions generated by corona discharge have to transport across the dust layer to migrate to the collection plate [22]. Therefore, the presence of dust layer can significantly influence the discharge characteristics of the ESPs. Meanwhile, the voltage of the dust layer surface will increase rapidly due to charge accumulation with increasing thickness, which weakens the electric field strength and ion charge density of the discharge space [23]. These may decrease the migration of charged particles to the collection plate and weaken the particle removal performance of the ESPs [24]. Therefore, the dust layer is one of the essential parameters affecting the particle removal efficiencies of ESPs and closely related to the deposition characteristics of charged particles. And it is also a critical issue that restricts the stable operation and wide industrial application of ESPs.

Given that this study is rather complicated but essential, numerous relevant experiments and numerical studies have been carried out to investigate the effect of the dust layer on particle removal in electric field. Gao et al. [25] investigated the effect of dust layer on particle removal and found that the removal efficiency of 10 μm particles decreased rapidly from 89.0 % without dust layer to 62.4 % at 80 kV applied voltage, 5 mm thickness and 10^{12} Ω·cm resistivity of the dust layer. Huang et al. [26] reported that the thickness of the dust layer can reach 3 mm, and the particle removal efficiency decreased by 13 % after an ESP continued to operate for five hours. With the charge generated by the discharge electrode continuously accumulating on the surface of dust layer, charged particles can cause gas breakdown within the dust layer when the electric field strength between particles exceeds the threshold of gas breakdown [27]. At this time, the corona discharge process of ESPs is extremely unstable and cannot operate normally, which is called the back corona [27–29].

Moreover, the particles deposited on the collection plate may return to the discharge space due to the entrainment effect of the flue gas, causing considerable degradation in the particle removal efficiency, which is called particle re-entrainment [30–32]. It is closely related to the deposition characteristics and adhesion force of charged particles. Blanchard et al. [33] concluded that there were significant differences in the particle accumulation morphology at different areas of the collection plate. The particles in the area directly facing the tip of the discharge electrode showed dendritic accumulation, and the dust layer was loose, which was easily entrained by the flue gas and returned to the discharge space. But the particle accumulation in other areas was denser. Zhu et al. [34] observed that the dust layer in the area directly facing the electrode tip was thicker in accumulation and gradually thinned along the direction of the flue gas. However, the re-entrainment mechanism of the deposited particle and its effect have not yet been clearly understood and identified.

In summary, several studies have been carried out on the gas breakdown and particle re-entrainment on the surface of dust layer. However, the deposition characteristics and re-entrainment mechanism of charged particles in electric field still remain unclear. And there is a lack of consideration on chain agglomerates of polarized particles.

In this study, a transparent ESP was designed to directly observe the dynamic process of charged particle deposition, clustering and gas breakdown in electric field. The polarization characteristics of the deposited particles in electric field were discussed. And the particle charging and migration performance at the moment of gas breakdown were systematically explored. Moreover, the countermeasures for optimizing the electric field and particle removal enhancement were proposed. These findings are crucial for the stable and efficient removal of particles from complex flue gas in various industries through electrostatic methods.

2. Experimental setup and method

2.1. Experimental system

Fig. 1 illustrates a schematic of the experimental system which mainly consists of five parts: a transparent ESP, a camera, a high-voltage power supply, and an electrostatic low-pressure particle impactor ($ELPI^+$).

The transparent ESP mainly consisted of flow channel, a discharge electrode and collection plate. The flow channel was made of PTFE and silica glass (Hengyang Optical Technology, China). And the length of the flue gas channel was 600 mm and the width was 50 mm [35]. Inside this ESP, the particle charging area was a needle-plate structure. Both the discharge electrode and collection plate were made of 316 L stainless steel. The tip cone angle and the radius of the top tip of the needle electrode were 30° and 25 μm, respectively. After each gas breakdown experiment, the discharge electrode was replaced to prevent tip oxidation from causing measure errors in subsequent experiments.

The collection plate was a smooth stainless-steel plate 50 mm in width and 200 mm in length. A baffle with a height of 5 mm was welded around the plate to conveniently lay the dust sample on the collection plate. Notably, there was a buffer area of 200 mm from the collection plate to both the inlet and outlet of the flue gas, which could effectively avoid the influence of velocity variations on the flow field in the observation area. To ensure sufficient electric field strength and ion charge density for gas breakdown on the surface of dust layer, the distance between the electrode tip and the collection plate was set to 25 mm.

The observation window was made of K9 optical glass (Hengyang Optical Technology, China) with a diameter of 50.8 mm. It was installed on the sidewall of the flue gas channel to observe the deposition performance of charged particles. To prevent the influence of electromagnetic waves generated by gas breakdown, a high-speed camera (X150, Thousand Eyes Wolf, China) with a resolution of up to 2560 × 1920 pixels and a stable digital single-mirror reflective camera (EOS 6D, Canon, Japan) with a wide-angle lens (RF24–105 mm, Canon, Japan) were used to record the dynamic process of particle clustering and gas breakdown in electric field.

A high-voltage power supply (SL60N600, Spellman, USA) was used for corona discharge with a maximum output voltage of 60 kV in this study. A high-voltage resistor ($R_2 = 5$ MΩ) was connected to the system to prevent high-voltage breakdown. To ensure the accuracy of the experiments, the voltage outputted from the high-voltage power supply was measured directly by a high-voltage probe (P150-G, Finechem, Japan). In addition, a voltage probe (TPP0500, Tektronix, USA) was used to measure the voltage across a constant value resistor ($R_1 = 5$ KΩ). The corona current can be obtained by Eq. (2). Due to its rapid response and high accuracy, an electrostatic low-pressure particle impinger (ELPI+, Dekati, Finland) connected to a vacuum pump (SV25B, Ernst Leybold, Ltd., Germany) was used to measure the concentration and charge of the particles in this study.

Previous studies has found that the particles from copper smelting plant were difficult to remove [36] and susceptible to cause the gas breakdown in ESPs. Therefore, the particles from copper smelting plant

were chosen for this study to investigate the dynamic process of particle deposition, clustering and gas breakdown in electric field. The mass concentration of particles in the flue gas was maintained at 260.0 mg/m^3. And the gas flow in the flue gas channel was kept at 1 m/s. The morphological characteristics of particles from copper smelting plant obtained by Scanning Electron Microscope (SEM) are illustrated in Fig. 2. The copper smelting particles in flue gas can be observed that they were susceptible to mutual adhesion and clustering, featuring irregular porous flocculent structures. Meanwhile, numerous submicron particles were prone to adhere to the surface of large size particles.

Before corona discharge of the transparent ESP, a dust layer with a thickness of 5 mm was laid on the collection plate, and the surface was scraped lightly with a ruler to ensure smoothness. Subsequently, the flue gas containing the particles from copper smelting plant began to enter the flow channel, and the power supply was quickly turned on after the mass concentration of particles was stabilized. The applied voltage was maintained at 20 kV. The charged particles in the flue gas rapidly moved toward the collection plate under the action of electric field force. And then the dynamic process of particle clustering and gas breakdown in electric field can be observed by a camera.

2.2. Analytical methods

In this study, the charging characteristics, mass concentration, and number concentration of the particles were obtained by ELPI$^+$. The relationship between the particle charge (q_p) and the fractional current can be calculated as follows:

$$q_p = I^* \Big/ \eta^* Q N_{outlet(i)} \tag{1}$$

where I^* represents the fractional current,η^* represents the particle charging efficiency for that size range measured by the ELPI$^+$, which is 100 % in this study [37], and Q represents the sampling flue gas flow in ELPI$^+$, and $N_{outlet(i)}$ represents the number concentration (cm^{-3}) of fractional particles at the outlet.

The corona current generated between the electrode tip and collection plate was expressed as:

$$I = U_1/R_1 \tag{2}$$

where U_1 represents the voltage across the constant value resistor (R_1 = 5 kΩ) measured by a voltage probe.

The voltage between the discharge electrode and collection plate can be calculated through U_2 measured by a high-voltage probe (the high-voltage probe divider ratio was 3000:1). The actual applied voltage in the ESP was calculated as follows:

$$U = U_2 - (R_1 + R_2) \times I = U_2 - U_1 \times (R_1 + R_2)/R_1 \tag{3}$$

where R_2 represents the protection resistor, R_2 = 5 MΩ.

The particle collection efficiency (η) was calculated as follows:

$$\eta = \left(\sum_{i=1}^{n} c_{inlet(i)} - \sum_{i=1}^{n} c_{outlet(i)} \right) \Big/ \sum_{i=1}^{n} c_{inlet(i)} \times 100\% \tag{4}$$

where $c_{inlet(i)}$ and $c_{outlet(i)}$ represent the fractional particle mass concentrations (mg/cm^3) at the outlet without and with corona discharge, respectively.

3. Results and discussion

3.1. Deposition performance of charged particles

The charged particles deposited on the collection plate interacted with each other, which may cause gas breakdown on the surface of deposited particles. To obtain deeper insight into the mechanism of particle clustering and gas breakdown in electric field, this section first investigated the deposition performance of charged particles on the collection plate. Fig. 3 shows the morphological photograph of the deposited particles after the power supply was turned on for 5 s. The growth sites of the chain agglomerates were strongly correlated with the distribution of the electric field on the surface of dust layer. The electric field strength was higher in the areas directly underneath the discharge electrode tips, and the polarization effect of the charged particles was more significant. The polarization force can overcome the gravity of the particles and the Coulomb repulsive force between the particles, causing the particles to agglomerate and attach to the surface above the chain agglomerates. The length of chain agglomerates observed in study can exceed 10 mm. This was obviously beyond the conventional understanding of the particle deposition process in ESPs.

Based on the abovementioned phenomenon, the particle polarization and formation mechanism of chain agglomerates during the corona discharge process is illustrated in Fig. 4.

The formation process of chain agglomerates in electric field can be divided into the following four steps in detail:

(a) The electric dipole was formed when the particles were placed in a high-voltage electric field. In other words, the positive and negative charges inside the particle moved apart due to the electric field force and redistributed on the particle surface to eliminate the potential difference inside the particle caused by the external electric field. Eventually, a certain amount of positive and negative charges was distributed on both sides of the particle along the electric field direction.

(b) Due to the contact charging mechanism, charge transfer occurred between the particles and the collection plate, which caused the

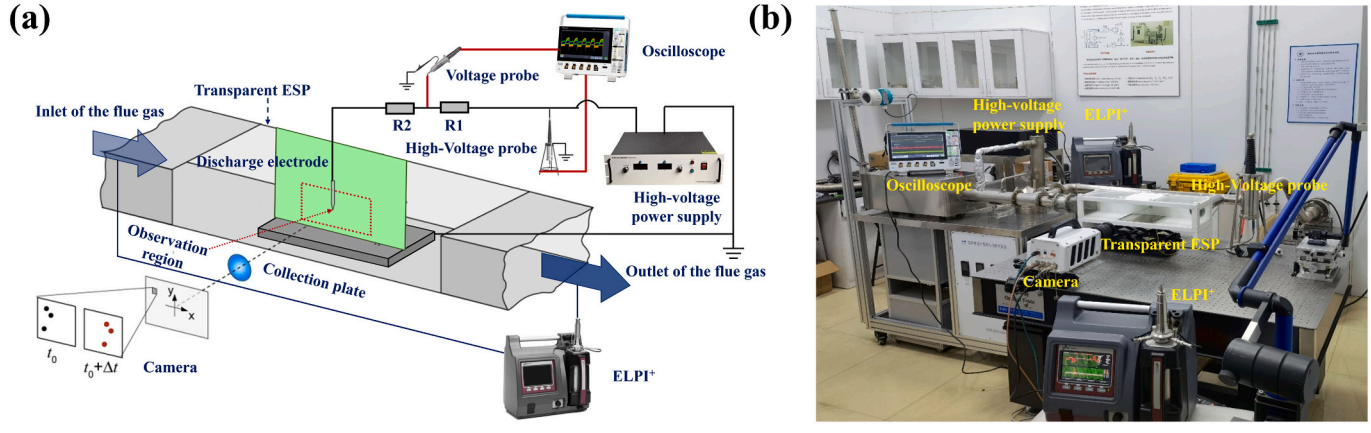

Fig. 1. Schematic of the experimental system: (a) schematic, (b) photograph.

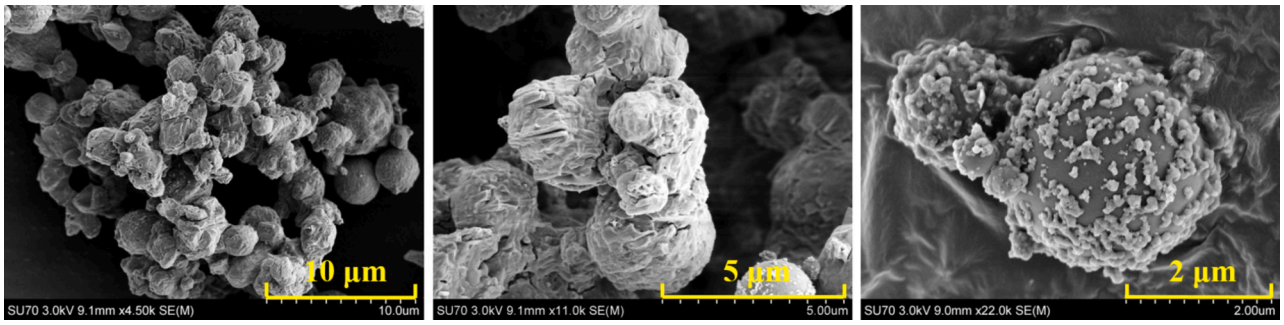

Fig. 2. The morphological characteristics of the deposited particles.

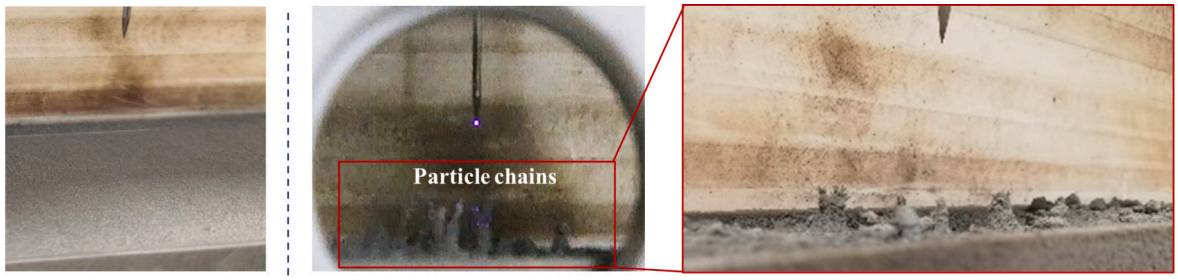

Fig. 3. Particles accumulated to form chain agglomerates in the electric field.

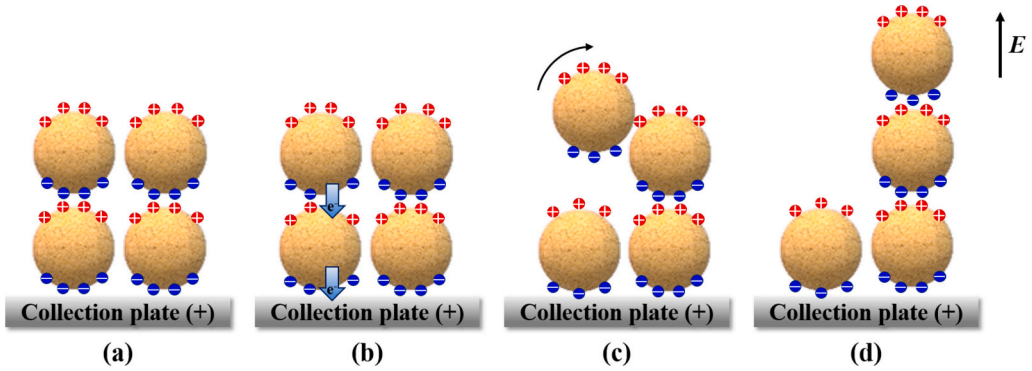

Fig. 4. Schematic diagrams of chain agglomerates formation in electric field.

deposited particles to carry some net charges. Meanwhile, the corona discharge also charged the particles, which further improved the net charge of deposited particles and enhanced particle polarization.

(c) Under the influence of net charges, the polarized particles on the surface of dust layer had a tendency to float upwards due to the electric field force caused by the applied electric field. And they were also attracted by the polarized electric field from the chain agglomerates.

(d) Under the action of the electric dipole moment, the attracted particles would rotate and move laterally, resulting in the particles clustering together along the electric field lines. The polarized particles around the particle chain were continuously attracted over time and eventually formed chain agglomerates consisting of multiple polarized particles.

3.2. Particle clustering and gas breakdown in electric field

Surface gas breakdown occurred on the surface of dust layer with increasing applied voltage, as shown in Fig. 5(a). When the applied voltage surpassed a threshold value, the surface gas breakdown rapidly transformed into interelectrode gas breakdown and caused a short circuit, as displayed in Fig. 5(b). It was observed that the surface gas breakdown mainly occurred at the top of the chain agglomerates rather than in the middle region. This was mainly due to the high curvature of the particle chain top, which caused higher surface charge density and electric field strength.

Fig. 6 illustrates the formation and fracture of chain agglomerates over time on the surface of dust layer. During the corona discharge process, the particle chains began to develop and grew up gradually with time. It was worth noting that the growth direction of the particle chains was not vertical to the collection plate but rather toward the electrode tip, which was almost parallel to the direction of electric field lines. This indicated that the electric field force played an important role in the formation of chain agglomerates.

When the particle chains grew up to approximately half the distance between the electrode tip and the collection plate, interelectrode gas breakdown suddenly occurred from the particle chains to electrode tip in this study. This phenomenon usually occurred without any precursor, and even the corona current had not yet fluctuated significantly.

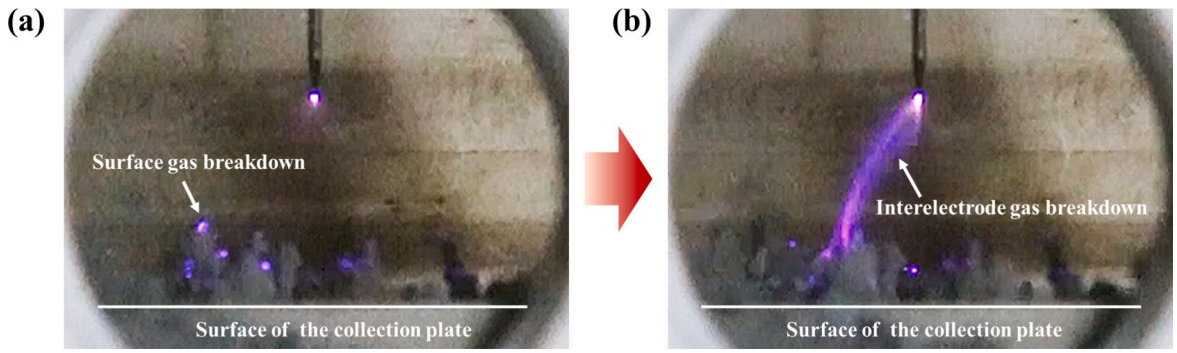

Fig. 5. Process of gas breakdown on the deposited particle surface: (a) surface gas breakdown (b) interelectrode gas breakdown.

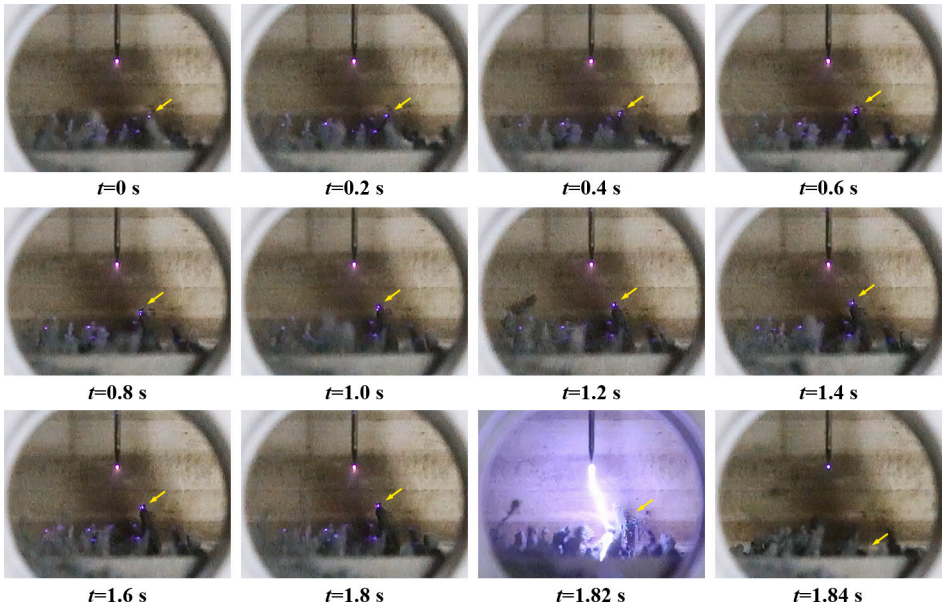

Fig. 6. Formation and fracture of chain agglomerates.

Therefore, the interelectrode gas breakdown had a certain randomness. The particle chains were broken after gas breakdown, and partial chain agglomerates re-entered into the flue gas. These particle chains may be scattered by the flue gas and produced fine particles with different sizes, which increased the fine particle concentrations at the outlet. Certainly, they might also be recaptured or quickly escape through the outlet. In addition, it is worth noting that gas breakdown also caused the eruption of particles from the dust layer, forming some craters there.

Based on the above results, it was shown that the growth of chain agglomerates was one of the essential reasons for interelectrode breakdown and particle re-entrainment in ESPs. In practical applications, the morphological characteristics of the deposited particles should be considered, especially for flue gas with a high mass concentration or highly adhesive particles. It was more likely to form longer and denser chain agglomerates in electric field, causing severe gas breakdown and particle re-entrainment in ESPs.

3.3. Particle charging and migration performance at the moment of gas breakdown

When gas breakdown occurred on the surface of dust layer, numerous positive ions generated by gas ionization were released into the discharge space under the action of the electric field force. Consequently, the particle charge in the flue gas would be changed, which might affect the efficient removal of particles in ESPs. To explore this question, real-time measurements of the particle charge were carried out at the outlet of the flue gas to obtain the particle charge of various sizes during the gas breakdown, as displayed in Fig. 7. During the gas breakdown, the negative charge of particles of all sizes decreased, and the charging characteristics of particles with sizes larger than 4.44 μm reversed from "negative" to "positive". This was mainly caused by the fact that the effective cross-sectional area of large-size particles was much larger which can capture more positive charge. For example, the average charge of 7.30 μm particle was changed from -1.61×10^{-16}C in typical condition to $+8.95 \times 10^{-17}$C in gas breakdown.

Fig. 8 shows the effect of gas breakdown on the particle number concentration at the outlet. Gas breakdown caused a significant increase in the outlet concentrations of particles of all sizes, especially for particles smaller than 0.12 μm and larger than 3.01 μm. For example, during gas breakdown, the number concentrations of 7.30 μm particles at the outlet could increase by 2.48 times. The increased outlet concentration of small-size particles was mainly due to the fact that gas breakdown significantly decreased the charge of small-size particles, which was not favorable for efficient particle removal. Meanwhile, the gas breakdown also caused the fragmentation of some submicron particles and produced more particles with smaller particle sizes. The increase in the outlet concentration of large-size particles was mainly due to the fracture of chain agglomerates, resulting in the particle re-entrainment.

Through a comprehensive analysis of particle charging and

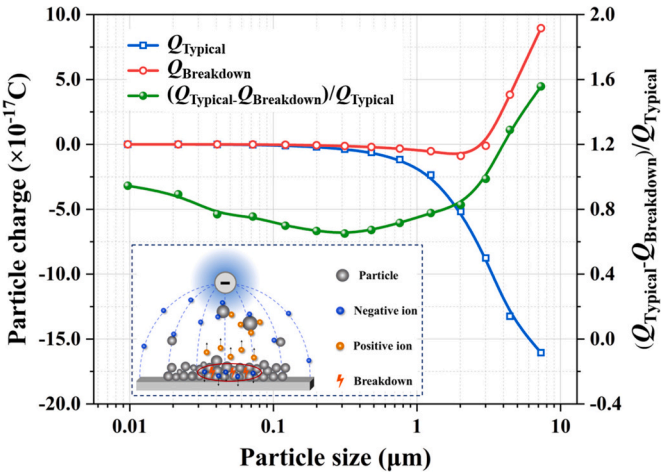

Fig. 7. Effect of gas breakdown on the particle charge.

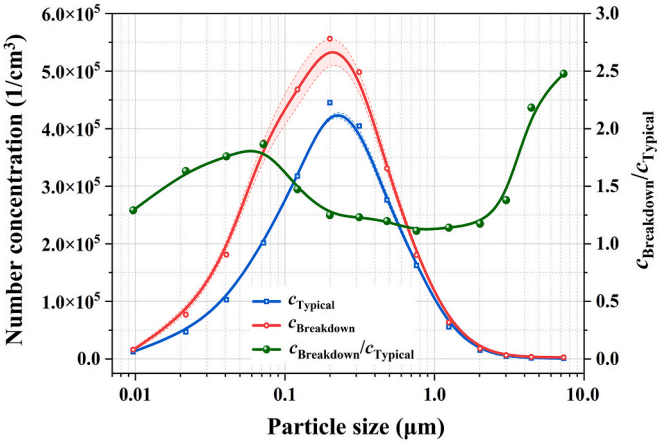

Fig. 8. Effect of gas breakdown on the particle number concentration at the outlet.

migration performance at the moment of gas breakdown, it was found that particle breakdown significantly challenged the efficient and stable operation of ESPs, especially with a high concentration of fine particles in flue gas or massive deposited particles on the surface of collection plate. On the one hand, gas breakdown could lead to the fracture of chain agglomerates on the surface of dust layer, causing particles re-entrainment in ESPs. On the other hand, it also decreased the space electric field and the particle charge due to the alteration of the particle charging characteristics. These two combined aspects caused a serious decrease in particle removal efficiency in the ESPs.

3.4. Countermeasures for optimizing the electric field and particle removal enhancement

Due to the high electric field strength within the near-plate region, the deposited particles can form chain agglomerates and further cause gas breakdown beginning from surface of the dust layer. Meanwhile, the high-speed ionic wind generated by corona discharge also exhibited a scouring effect on the collection plate, causing the re-entrainment of broken particle chains from surface of the dust layer. Hence, particle clustering and gas breakdown on the surface of dust layer posed a serious challenge to the operation efficiency and stability of the ESPs. To overcome these drawbacks, this study proposed a novel collection plate (perforated plate), as shown in Fig. 9. The main principle of this collection plate was to optimize the space flow characteristics of the ESPs and the electric field intensity distribution within the near-plate region by installing a perforated plate close to the common collection plate (flat plate). Due to its better discharge performance, a spike electrode and an arista electrode were chosen as discharge electrodes in this section.

The characteristics of the electric field distribution near the electrode tips with the flat plate and the perforated plate were presented in Fig. 10. The results revealed that the presence of the perforated plate significantly increased the electric field strength between the electrode tip and the collection plate, which can enhance the deposition process of charged particle. Meanwhile, the perforated plate could also optimize the electric field distribution within the near-plate region. The electric field strength near the perforated plate dropped rapidly from 6.43×10^5 V/m to below 2.51×10^4 V/m, which greatly minimized the possibility of gas breakdown on the surface of dust layer. Meanwhile, the deposited particles were also not easily polarized to form chain agglomerates in such a low electric field environment.

The current-voltage characteristics of the corona discharge for four ESP configurations is shown in Fig. 11. The slope of the corona current increased significantly with increasing applied voltage after installing a perforated plate. Although the breakdown voltage of ESPs decreased with the perforated plate, the maximum corona currents of the spike electrode and the arista electrode still increased by 30.3 % and 15.3 %, respectively. On the one hand, higher corona current enhanced the particle charging process, especially for particles smaller than 1.0 μm in diameter. On the other hand, it also improved the role of ionic wind in promoting particle migration.

The effect of a perforated plate on particle removal was investigated under various applied voltages, as presented in Fig. 12. The particle removal efficiencies of two types of discharge electrodes with a perforated plate increased at various applied voltages. For the spike electrode and arista electrode, the maximum removal efficiency of the particles increased by 11.5 % and 6.1 %, respectively. Compared with that of the spike electrode, the increase in the particle removal efficiency of the arista electrode was relatively small, which presumably might be related to the strength of the ionic wind in the discharge space. The stronger ionic wind generated by corona discharge for the spike electrodes can

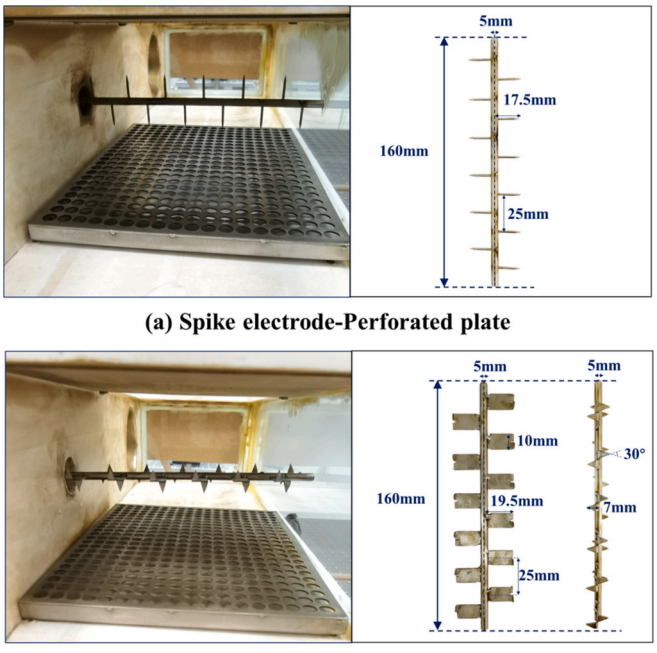

Fig. 9. Electrostatic precipitator equipped with a perforated plate: (a) spike electrode-perforated plate, (b)arista electrode-perforated plate.

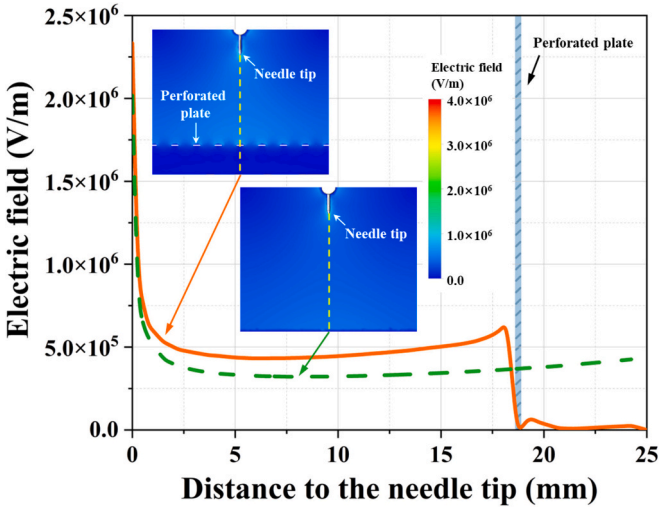

Fig. 10. Effect of the perforated plate on the electric field distribution.

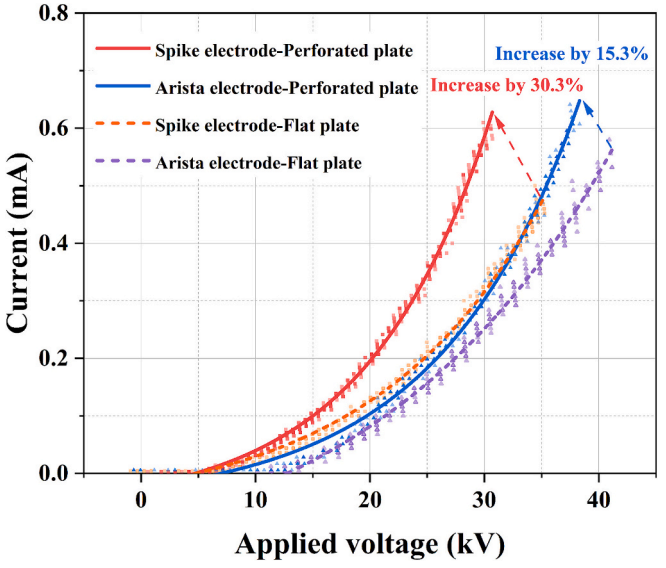

Fig. 11. Current-voltage characteristics of the corona discharge for four ESP configurations.

promote the migration of particles toward the collection plate and optimize the space flow field to prevent the excessive accumulation of charged particles. While the ionic wind generated by the arista electrode disturbed the flow field weakly, the charged particles were prone to accumulate on collection plate. The interactions between the accumulated charged particles caused local gas breakdown at high applied voltages, which was the main reason for the increase first and subsequent decrease in the particle removal efficiency of the arista electrode.

A comparison of the particle mass concentrations for the four ESP configurations under various applied voltages is illustrated in Fig. 13. It can be seen that the perforated plate can be effectively inhibited particle re-entrainment. The mass concentrations of particle re-entrainment decreased from 71.6 mg/m^3 to 10.6 mg/m^3 for the spike electrode and from 42.2 mg/m^3 to 8.8 mg/m^3 for the arista electrode at an applied voltage of 30 kV. In other word, for the spike electrode and the arista electrode, the mass concentrations of particle re-entrainment decreased by 85.2 % and 79.1 %, respectively. Moreover, the increase in the applied voltage had no significant influence on particle re-entrainment, which means that the amount of re-entrainment particles at high applied voltages was also within the controllable range. In practical

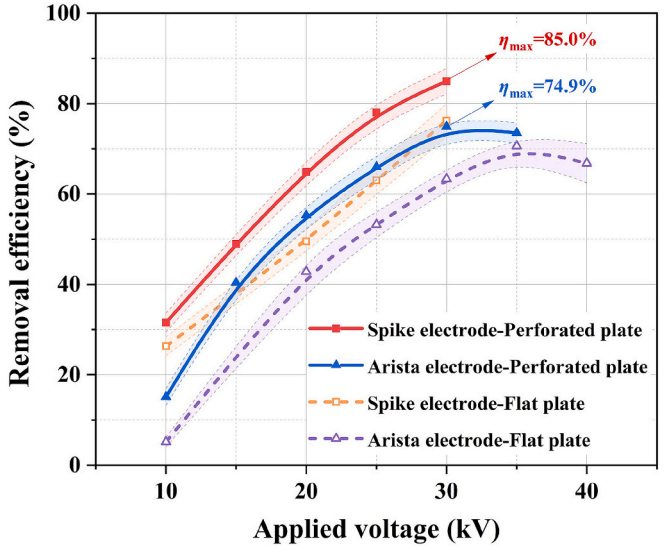

Fig. 12. Enhanced particle removal performance due to the installation of a perforated plate.

applications, the perforated plate can also be replaced by a metal mesh according to the site conditions and operation requirements. The basic principle of collection plate optimization was to create a low electric field strength and low space velocity environment within the near-plate region.

4. Conclusion

In this study, a transparent ESP was designed to investigate the dynamic process of charged particle deposition, clustering and gas breakdown in electric field. The particle charging and migration performance at the moment of gas breakdown were systematically discussed. Moreover, relevant countermeasures for optimizing the electric field and enhancing particle removal were proposed. The detail conclusions were drawn as follows:

(1) The deposited particles will aggregate and gradually grow in chains under the combined effects of electric field force and polarization force when charged particles entered in high-voltage electric field. The growth sites of the chain agglomerates were strongly correlated with the distribution of the electric field strength on the surface of dust layer. The length of chain agglomerates observed in this study can exceed 10 mm.

(2) Surface gas breakdown occurred at the top of the chain agglomerates and can spread rapidly transformed into interelectrode gas breakdown with increasing applied voltage, causing particle re-entrainment in ESPs. Moreover, the surface gas breakdown mainly occurred at the top of the chain agglomerates due to higher surface charge density and electric field strength.

(3) Gas breakdown significantly affected the particle charging characteristics and concentrations at the outlet. During gas breakdown, the average charge of 7.30 μm particles was changed from -1.61×10^{-16}C in normal to $+8.95 \times 10^{-17}$C. Moreover, the number concentration of 7.30 μm particles at the outlet could increase by 2.48 times in gas breakdown.

(4) A perforated plate was proposed to inhibit the gas breakdown and re-entrainment of deposited particles. For the spike electrode and the arista electrode, the maximum removal efficiency increased by 11.5 % and 6.1 % when perforated plate installation, and the mass concentrations of particle re-entrainment decreased by 85.2 % and 79.1 %, respectively.

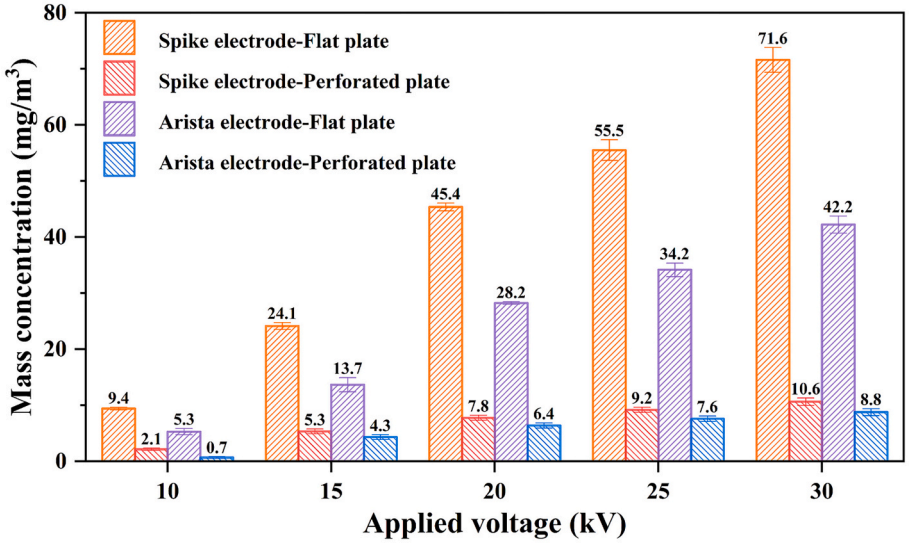

Fig. 13. Inhibition of re-entrainment due to the installation of perforated plate.

CRediT authorship contribution statement

Yifan Wang: Writing – original draft, Visualization, Methodology, Investigation, Conceptualization. **Meng Yang:** Writing – review & editing, Writing – original draft, Methodology, Formal analysis. **Zhicheng Wu:** Validation, Supervision, Conceptualization. **Lingyu Shao:** Investigation, Data curation. **Libin Yu:** Visualization, Data curation. **Yongxin Zhang:** Investigation. **Zhengda Yang:** Validation. **Yingchun Wu:** Supervision. **Chenghang Zheng:** Resources, Project administration, Funding acquisition. **Xiang Gao:** Supervision, Resources, Funding acquisition.

Declaration of competing interest

None.

Data availability

Data will be made available on request.

Acknowledgments

This work was supported by the National Natural Science Foundation of China (52076191, 52306279), the "Pioneer" and "Leading Goose" R&D Program of Zhejiang (2023C03008), the China Postdoctoral Science Foundation under Grant No. 2024T170765, and the Fundamental Research Funds for the Central Universities (2022ZJJH02-03).

References

[1] Z. Yu, J. Liu, R. Shen, G. Li, C. Lv, M. Zhu, An efficient thumbtack-cylinder type wet electrostatic precipitator for moxa smoke aerosol control, Powder Technol. 424 (2023) 118562.
[2] A. Jaworek, A.T. Sobczyk, A. Krupa, A. Marchewicz, T. Czech, L. Śliwiński, Hybrid electrostatic filtration systems for fly ash particles emission control. A review, Sep. Purif. Technol. 213 (2019) 283–302.
[3] D. Zhang, X.-D. Huang, J.-T. Zhong, L.-F. Guo, S.-Y. Guo, D.-Y. Wang, C.-H. Miao, X.-L. Zhang, X.-Y. Zhang, A representative CO2 emissions pathway for China toward carbon neutrality under the Paris Agreement's 2 °C target, Adv. Clim. Chang. Res. 14 (2023) 941–951.
[4] M.M. Badami, R. Tohidi, M. Aldekheel, V.J. Farahani, V. Verma, C. Sioutas, Design, optimization, and evaluation of a wet electrostatic precipitator (ESP) for aerosol collection, Atmos. Environ. 308 (2023) 119858.
[5] J. Zhao, Z. Liu, B. Wang, Q. Song, Y. Cai, A.M. Khan, Y. Wan, X. Ren, A comprehensive review of generating, monitoring, evaluating, and controlling particle emissions during machining process, J. Manuf. Syst. 70 (2023) 395–416.
[6] Z. Sun, L. Yang, S. Chen, L. Bai, X. Wu, Promoting the removal of fine particles and zero discharge of desulfurization wastewater by spray-turbulent agglomeration, Fuel 270 (2020) 117461.
[7] S. Kim, K. Park, C. Choi, M.Y. Ha, D. Lee, Removal of ultrafine particles in a full-scale two-stage electrostatic precipitator employing a carbon-brush ionizer for residential use, Build. Environ. 223 (2022) 109493.
[8] Y. Wang, Y. Lu, C. Huang, Z. Liu, Z. Li, Z. Chen, F. Fang, Effects of the addition of arch-supplied secondary air on the performance of the Foster wheeler down-fired boiler: air/particle flow, combustion and NOx emissions, Fuel 371 (2024) 132074.
[9] P. Mangaraj, S.K. Sahu, G. Beig, Development of emission inventory for air quality assessment and mitigation strategies over most populous Indian megacity, Mumbai, Urban Clim. 55 (2024) 101928.
[10] Y. Zhou, Y. Liu, Z. Shi, X. Li, M. Yu, Enhanced size-dependent efficiency of removal of ultrafine particles: new solution of two-stage electrostatic precipitator with thermophoresis, Sep. Purif. Technol. 346 (2024) 127479.
[11] Z. Feng, J. Yang, J. Zhang, Numerical optimization on newly developed electrostatic enhanced pleated air filters for efficient removal of airborne ultra-fine particles: towards sustainable urban and built environment, Sustain. Cities Soc. 54 (2020) 102001.
[12] M. Dong, F. Zhou, Y. Shang, S. Li, Numerical study on electrohydrodynamic flow and fine-particle collection efficiency in a spike electrode-plate electrostatic precipitator, Powder Technol. 351 (2019) 71–83.
[13] C. Qi, X. Yang, J. Yao, W. Wang, Y. Dong, X. Xu, L. Cui, Effect of charged spray evaporation of desulfurization wastewater on fine particle removal efficiency of electrostatic precipitator, Process. Saf. Environ. Prot. 179 (2023) 99–107.
[14] Y. Chang, P. Jia, L. Shi, X. Xiang, Corona discharging and particle collection of bipolar transverse plate ESP, J. Electrost. 96 (2018) 104–110.
[15] Y. Wang, H. Zhang, W. Gao, L. Shao, Z. Wu, Z. Zhao, C. Ge, D. Hu, C. Zheng, X. Gao, Improving the removal of particles via electrostatic precipitator by optimizing the corona wire arrangement, Powder Technol. 388 (2021) 201–211.
[16] O. Molchanov, K. Krpec, J. Horák, L. Kubonová, F. Hopan, J. Ryšavý, Combined control of PM and NOx emissions by corona discharge, Sep. Purif. Technol. 345 (2024) 127359.
[17] A. Jaworek, A. Marchewicz, A.T. Sobczyk, A. Krupa, T. Czech, Two-stage electrostatic precipitator with dual-corona particle precharger for PM2.5 particles removal, J. Clean. Prod. 164 (2017) 1645–1664.
[18] M. Jędrusik, A. Świerczok, The correlation between corona current distribution and collection of fine particles in a laboratory-scale electrostatic precipitator, J. Electrost. 71 (2013) 199–203.
[19] J.H. Chung, K.H. Kim, D.K. Sohn, H.S. Ko, Numerical study on staggered needle-plate electrode configuration for improved particulate matter collection in electrostatic precipitator, Powder Technol. 443 (2024) 119865.
[20] O. Molchanov, K. Krpec, J. Horák, L. Kuboňová, F. Hopan, Comparison of methods for evaluating particle charges in the electrostatic precipitation of fly-ash from small-scale solid fuel combustion, Sep. Purif. Technol. 248 (2020) 117057.
[21] D. Patiño, B. Crespo, J. Porteiro, E. Villaravid, E. Granada, Experimental study of a tubular-type ESP for small-scale biomass boilers. Preliminary results in a diesel engine, Powder Technol. 288 (2016) 164–175.
[22] W. Xiong, Z. Lin, W. Zhang, T. Chen, C. Zhao, Experimental and simulation studies on dust loading performance of a novel electrostatic precipitator with dielectric barrier electrodes, Build. Environ. 144 (2018) 119–128.
[23] C. Zheng, H. Zhang, X. Liu, Y. Wang, W. Gao, H. Zheng, D. Sun, X. Gao, Effect of dust layer in electrostatic precipitators on discharge characteristics and particle removal, Fuel 278 (2020) 118335.

[24] C. Zheng, C. Liang, S. Liu, Z. Yang, Z. Shen, Y. Guo, Y. Zhang, X. Gao, Balance and stability between particle collection and re-entrainment inawide temperature-range electrostatic precipitator, Powder Technol. 340 (2018) 543–552.
[25] W. Gao, Y. Wang, H. Zhang, B. Guo, C. Zheng, J. Guo, X. Gao, A. Yu, A numerical investigation of the effect of dust layer on particle migration in an electrostatic precipitator, aerosol air, Qual. Res. 20 (2020) 166–179.
[26] S.-H. Huang, C.-C. Chen, Loading characteristics of a miniature wire-plate electrostatic precipitator, Aerosol Sci. Technol. 37 (2003) 109–121.
[27] H. Zhang, Y. Wang, W. Gao, Z. Wu, Z. Yang, Y. Yang, W. Wu, C. Zheng, X. Gao, Minimizing the adverse effects of dust layer on the particle migration in electrostatic precipitator under various temperature, Fuel Process. Technol. 213 (2021) 106659.
[28] Y. Shi, M. Fang, Q. Wang, K. Yan, J. Cen, Z. Luo, Enhanced high-temperature particle capture through an electrostatic precipitator with assistant electrodes, Sep. Purif. Technol. 324 (2023) 124550.
[29] A. Krupa, J. Podliński, J. Mizeraczyk, A. Jaworek, Velocity field of EHD flow during back corona discharge in electrostatic precipitator, Powder Technol. 344 (2019) 475–486.
[30] Y. Shi, C. Li, M. Fang, J. Cen, Q. Wang, K. Yan, Numerical investigation of particle re-entrainment mechanism and its suppression strategy in the high-temperature electrostatic precipitator, Powder Technol. 437 (2024) 119538.
[31] Y. Zhu, Y. Zhang, X. Yang, S. Tao, M. Chen, W. Shangguan, Operando investigation of particle re-entrainment mechanism in electrostatic capture process on the lab-on-a-chip, J. Environ. Sci. 136 (2024) 337–347.
[32] Q.-Z. Xue, T.-Y. Wen, Separating Al2O3 particles from high-speed flue gas by an induced flow recirculation in two-stage electrostatic precipitator, Sep. Purif. Technol. 234 (2020) 116105.
[33] D. Blanchard, P. Atten, L.M. Dumitran, Correlation between current density and layer structure for fine particle deposition in a laboratory electrostatic precipitator, IEEE Trans. Ind. Appl. 38 (2002) 832–839.
[34] Y. Keping, Characteristics of collected dust layer in a laboratory electrostatic precipitator, Sci. Technol. Rev. 26 (2008) 30–33.
[35] Y. Wang, M. Yang, L. Shao, Z. Wu, W. Liu, Y. Chen, C. Zheng, X. Gao, Enhancing fine particle removal by electrostatic precipitation from flue gas with a high PM concentration: effect of various electrode configurations, Sep. Purif. Technol. 353 (2025) 128459.
[36] J. Zhang, X. Sun, J. Deng, G. Li, Z. Li, J. Jiang, Q. Wu, L. Duan, Emission characteristics of heavy metals from a typical copper smelting plant, J. Hazard. Mater. 424 (2022) 127311.
[37] A. Järvinen, M. Aitomaa, A. Rostedt, J. Keskinen, J. Yli-Ojanperä, Calibration of the new electrical low pressure impactor (ELPI$^+$), J. Aerosol Sci. 69 (2014) 150–159.